Dalton Transactions

Accepted Manuscript

This is an *Accepted Manuscript*, which has been through the Royal Society of Chemistry peer review process and has been accepted for publication.

Accepted Manuscripts are published online shortly after acceptance, before technical editing, formatting and proof reading. Using this free service, authors can make their results available to the community, in citable form, before we publish the edited article. We will replace this *Accepted Manuscript* with the edited and formatted *Advance Article* as soon as it is available.

You can find more information about *Accepted Manuscripts* in the Information for Authors.

Please note that technical editing may introduce minor changes to the text and/or graphics, which may alter content. The journal's standard Terms & Conditions and the Ethical guidelines still apply. In no event shall the Royal Society of Chemistry be held responsible for any errors or omissions in this *Accepted Manuscript* or any consequences arising from the use of any information it contains.

ROYAL SOCIETY OF CHEMISTRY

www.rsc.org/dalton

Please do not adjust margins

Journal Name

ARTICLE

One-pot environmental friendly amino acid mediated synthesis of N-doped graphene-silver nanocomposites with enhanced multifunctional behavior

Received 00th January 20xx,
Accepted 00th January 20xx

DOI: 10.1039/x0xx00000x

www.rsc.org/

Mahima Khandelwal and Anil Kumar*

The present paper reports one-pot synthesis of N-doped graphene-Ag nanocomposites (N-GrAg) involving *in-situ* generation of Ag nanoparticles (NPs). The simultaneous reduction of GO and Ag^{+} to produce N-GrAg has been achieved under mild reaction conditions using environmental benign reducing agent, glycine in aqueous medium without adding any external stabilizer. XRD and SAED analyses revealed the presence of Ag in fcc structure. HRTEM analysis shows the 'd' spacing of 0.236 nm corresponding to the highest intense (111) reflection of Ag matching to the fcc structure. The N-doping of graphene and its uniform decoration by Ag NPs (with an av. dia. of 17.5 nm) having relatively low surface atomic % of Ag (0.309) is evidenced by TEM and XPS analyses. Raman spectroscopy has also revealed the decoration of N-Gr with Ag NPs resulted in the enhancement of the D and G bands by about 365 %. The presence of Ag in N-GrAg prevents the folding of graphene sheet as was revealed by TEM analysis. The supramolecular interactions of Ag with different moieties of N in N-GrAg was evidenced by IR, ^{13}C NMR and XPS analyses, which resulted in the enhancement of its surface area and electrical conductivity as compared to that of N-Gr. The presence of Ag NPs on N-Gr increased the current response in cyclic voltammetry by more than seven fold as compared to that of N-Gr. These nanocomposites exhibited fairly high SERS activity for 4-aminothiophenol, employed as the probe molecule and allowed its detection at 50 nM concentration even for the fairly small sized Ag NPs used in the present work.

Introduction

Research on graphene is drawing increasing attention due to their optical, mechanical, electrical, electronic and electrochemical properties.[1,2] The doping of heteroatoms into the graphene lattice is expected to bring a change in its structural and electronic behaviour possibly due to the polarization, thereby, altering its optical, electrical, electronic, magnetic and electrochemical properties.[3-5] Several heteroatoms such as B, P, S and N have been explored extensively which resulted in the enhancement of these features.[3-5] Among these heteroatoms, the doping of N is of significant interest because of its electron rich nature, comparable size to that of C and high electronegativity of N (3.04 on pauling scale) than that of C (2.55 on the Pauling scale) which might provide an appropriate location to fit into the graphene lattice. It has been observed that doping of N yields different bonding configurations namely pyridinic-N, pyrolic-N, quaternary-N, graphitic-N, and interstitial/adatoms with carbon in the graphene lattice and expected to influence the charge carrier mobility and electrical properties of pristine graphene significantly by opening its band gap and thereby creating defects.[3,6,7] Moreover, the doping of N has been widely explored for manipulating the electrochemical behavior by improving the electrical conductivity and wettability at the interface of electrolyte and electrode.[6,8,9]

Hitherto, a number of reducing agents have been used for the N-doping of graphene and most of these reagents (such as hydrazine, ammonia, hexamethyltetraamine, dicyandiamide and hydroxylamine)[10-14] are corrosive. In the recent past, a number of environmental friendly reducing agents including amino acids have also been investigated to produce N-doped graphene.[15-18] The morphological and physicochemical features of N-doped graphene could further be improved or modified by forming its nanocomposites with different metal nanoparticles (NPs). Among different metal NPs (Pd, Pt, Au and Ag),[19,20] Ag being economical and electrically conducting is largely used in microelectronics and LED devices for making electrical contacts.[21] Silver electrodes are relatively expensive and it would be desirable to replace them by fabricating Ag coated graphene electrodes. Graphene-Ag nanocomposites have also been used for catalysis and sensors applications.[22-23]

In literature N-doped graphene-Ag nanocomposites have been synthesized using both hazardous and environmental friendly reducing agents.[24-28] The presence of Ag NPs on N-doped graphene sheet would allow their interaction with N as well as their immobilization may also prevent the aggregation of graphene sheet by involving supramolecular interaction(s)

Department of Chemistry, Indian Institute of Technology Roorkee, Roorkee-247667,India. E-mail: anilkfcy@iitr.ac.in; akmshfcy@gmail.com; Fax: +91 1332 273560; Tel: +91 1332 285799

† Electronic Supplementary Information (ESI) available: See
DOI: 10.1039/x0xx00000x

Dalton Transactions Accepted Manuscript

Please do not adjust margins

with its delocalized π bonds. It is thus expected to result in an increase in its surface area besides enhancing the electrical conductivity, chemical stability, thermal stability, catalytic activity and electrochemical behavior. Such nanocomposites have been used as SERS substrate for the detection of various probe molecules[25,28] and also demonstrate their significant potential for applications in supercapacitor(s), electrochemical sensing and catalysis.[24,29,30]

Amino acids, being environmentally benign, have been used in the past to reduce graphene oxide to produce N-doped graphene.[15,16,27,28] As regards to the amino acid mediated synthesis of N-doped graphene-Ag nanocomposites, we have come across two reports employing glycine and arginine as reducing agents.[27,28] Mayavan *et al.*[27] have employed glycine as a reducing agent containing GO:Gly:Ag in the mass ratio (1:2:2) in aqueous medium. The resulting mixture was sonicated for 2 h followed by its gradual heating from room temperature to 500 ^{0}C under Ar atmosphere at 2 ^{0}C/min and was maintained at this temperature for 2 h. In another report[28] using arginine as a reducing agent, microwave induced (2.45 GHz, 900 W) reduction of GO was performed employing high concentration Ag^+ (100 mM). However, these nanocomposites have not been investigated for their multifunctional features such as electrical and electrochemical behavior.

In the present work, we have carried out simultaneous reduction of GO and its decoration with Ag NPs to produce N-doped graphene-silver nanocomposites under mild conditions of temperature and pH in aqueous medium using glycine as a environmental benign reducing agent. The as synthesized nanocomposites exhibit fairly high surface area with enhanced conductivity and electrochemical features as compared with that of N-doped graphene. These nanocomposites also showed fairly high SERS activity for the detection of 4-ATP as a probe molecule. In comparison to the previous report on arginine mediated synthesis of graphene-Ag nanocomposites, the present system employs fairly low concentration of Ag^+ and has demonstrated very similar SERS activity. To the best of our knowledge, this is the first report on these nanocomposites using environmentally benign conditions for the synthesis, analyzing the nature of interaction among different components and exploring their multifunctional features.

Experimental Section

Materials Used

Natural graphite flakes (+75 mesh) (Aldrich); 4-aminothiophenol (4-ATP) (Sigma-Aldrich); hydrogen peroxide (30%), hydrochloric acid, potassium permanganate, phosphorous pentoxide (s-d Fine Chemicals Ltd.); silver nitrate (AgNO3) (99.9%), potassium persulphate, potassium nitrate, dimethylformamide (DMF) (Merck); sulphuric acid (Thomas Baker); glycine and sodium hydroxide pellets (Himedia); ethanol (Changshu Yangyuan chemical Co., Ltd.). All reagents used were of analytical grade and were not purified any further. Dialysis tubing (seamless cellulose tubing) / closures were procured from Sigma. All solutions were prepared freshly in deionised water (DIW) (Bedford, MA, USA).

Equipment

The optical absorption spectra of the samples were recorded in the UV-Visible range (200 – 800 nm) on a Shimadzu UV2100 spectrophotometer using a quartz cuvette having a path length of 1 mm. Zeta (ζ) – potential measurement was performed on a Malvern Instruments, Nano-ZS90 (Zetasizer Nanoseries) equipped with a HeNe laser (632.8 nm) as the light source. Raman measurements were performed on a Renishaw inVia Raman spectrometer (serial no. 021R88) using argon ion laser as the source of excitation (514 nm) equipped with the confocal microscope having different objective lenses and thermo- electric cooled charge-coupled device (CCD) detector. X-ray diffraction patterns were recorded on a Bruker AXS D8 Advance X-ray diffractometer (XRD) in the 2θ range of 5 to 85^0 at a scan rate of 0.3^0 / step using Cu Kα radiation (1.5418 Å) as the source for X – rays at an AC voltage of 40 kV and electron probe current of 30 mA. The surface topography of the samples was analyzed by recording their two - dimensional images on an atomic force microscope (AFM, NTEGRE (NT-MDT)) equipped with NOVA software in a semi-contact mode. It has a resolution of 0.2 and 0.04 nm along the x-y axes and z-axis, respectively. The surface morphologies were further analyzed by using digital field emission scanning electron microscope (FE-SEM) QUANTA 200-FEG equipped with CCD camera. Elemental analysis at desired locations and mapping of the FESEM micrographs were performed by using energy dispersive x-ray analysis (EDAX) accessories procured from AMETEK materials analysis division. Data of these measurements was analyzed by using Aztec energy analysis software. Transmission electron micrographs (TEM), and selected area electron diffraction (SAED) were measured on a FEI- Tecnai G2 20 S-TWIN at an operating voltage of 200 kV equipped with CCD camera having different magnifications up to 1,100,000x. Fourier transform infrared (FTIR) spectra of the solid samples were recorded on a Thermo Nicolet Nexus (FTIR) spectrophotometer in the mid IR range of 4000 - 500 cm^{-1} in KBr medium and the data were processed by using OMNIC v6.1 software. X-ray photoelectron spectroscopy (XPS) measurements were recorded on an Omicron NanoTechnology instrument using the Mg K_α energy source. Thermogravimetric (TGA) analysis was carried out in the N_2 atmosphere on a SII TG/DTA 6300 EXSTAR at a heating rate of 10 °C/ min in the temperature range of 25 – 800 °C. The ^{13}C solid-state direct single pulse magic angle spinning (MAS) Nuclear Magnetic Resonance (NMR) spectra were recorded on a JEOL 400 MHz NMR spectrometer (Model ECX 400 II). The samples were packed into 4 mm rotor and the spectra were recorded at a spinning speed of 12 kHz using 10 s relaxation delays and 2.4 μs 90^0 pulse exciting over a bandwidth of 100 MHz without decoupling and averaged out for more than 3000 scans. The reference for ^{13}C spectrum was solid adamantane (29.4 ppm) based on trimethylsilane scale. Current-voltage (I-V) measurements were performed on the Keithley 2400 source meter using four probe method at room temperature and this system was procured from Photo Emission Tech. Inc., USA. Five point BET measurements were recorded using Autosorb-iQ (Quantachrome Instruments) at 77 K. Electrochemical measurements were performed at room temperature on a

Dalton Transactions Accepted Manuscript

This journal is © The Royal Society of Chemistry 20xx

computer controlled CHI760E electrochemical workstation (CH Instruments, USA) using a standard three electrode configuration consisting of glassy carbon electrode (GCE) of 3 mm diameter (0.07065 cm^2 area) as a working electrode, Pt wire as a counter electrode and Ag/AgCl (3M NaCl) as a reference electrode. Cyclic Voltammetry (CV) measurements were performed in the potential window of 0 – 0.8 V. The electrochemical impedance spectroscopy (EIS) measurements were performed in the frequency range of 0.1 Hz – 10 kHz with an amplitude voltage of 10 mV at an open circuit potential. The reactions at 95 ^{0}C were performed by using refrigerated circulating water bath from Lab companion (Model RW- 0525G). The pH of the solutions was maintained by using Toshniwal digital pH meter (Model CL 54 +). The centrifugation of the samples was performed on a REMI microprocessor research compufuge (Model PR-24) at a speed of 14 000 rpm. The samples were dried in a vacuum oven procured from Labtech, Daihan Labtech Co. Ltd.

Methodology

For Raman measurements, the samples were drop casted on the glass plate and then dried under ambient conditions. The dried glass plate was then placed underneath the 50x objective lens (0.75 nm NA) having the spectral resolution of 0.5 - 1 cm^{-1} in Raman shift and these measurements were recorded in the wavenumber range of 500 - 3500 cm^{-1}. In order to avoid any damage and changes in the sample, all measurements were performed at low laser power of 0.5 mW for an exposure time of 30 s. Each time prior to use, the system was calibrated by running the internal silicon reference at 520 cm^{-1}. For AFM analysis, samples were prepared by applying a drop of dilute sample on the clean glass plate followed by its drying under ambient conditions. For recording the AFM images the scanning frequency was varied in the range of 1.56 to 3.13 Hz at room temperature. From these images, the surface height along a particular line at different locations was measured by using NOVA software. For FESEM analysis, samples were prepared by sticking the pinch of solid sample on the double sided tape which is fixed on the aluminium stub. In order to make the surface of these samples conducting the samples was sputtered with gold and then the images were recorded by applying an acceleration voltage of 20 kV. For TEM analysis, a drop of the dilute sample was applied on a carbon coated copper grid G-200 (size 3.05 mm). The grid was subsequently dried in dark in order to evaporate the remaining moisture prior to its analysis at room temperature. Specific surface area, average pore diameter and pore size distribution were analyzed by using Brunauer–Emmett–Teller (BET) equation and density functional theory (DFT) method from NovaWin software. For I-V measurements, the film was prepared by applying the drop of liquid sample on transparent conducting indium titanium oxide substrate. The electrical contacts were made by using silver paste. The thickness of the N-Gr and N-GrAg films were estimated to be 5 and 4 µm, respectively. The resistivity was calculated by using the below given equation (1):[31]

$$\rho = (\pi/\ln 2)(V/I) \quad (1)$$

Where, ρ (Ω cm) is the resistivity, t (cm) is the thickness of the samples, V (V) is the applied potential and I (A) is the current flowing through the material. The conductivity (σ) can be calculated by using σ = 1/ ρ (S/cm). The specific capacitance (C_s) (F/g) from CV curves was calculated by using the below given equation (2):[31]

$$\frac{1}{2m \cdot \Delta V \cdot s}\left(\int_{0.8}^{0} idV + \int_{0}^{0.8} idV\right) \quad (2)$$

Where, m (g) denotes the mass of the active material applied on the electrode, ΔV (V) denotes the change in potential window, s (mV/s) is the scan rate and $\int_{0.8}^{0} idV + \int_{0}^{0.8} idV$ (A) denotes the total current obtained by the integration of positive and negative sweep in cyclic voltammetry.

The samples were dried in a vacuum oven at 50 ^{0}C for 12 h and were used as such for the measurements of XRD, FTIR, XPS and ^{13}C MAS NMR. For BET analysis, pellets of about 1-2 mm thickness were prepared using hydraulic press by applying a pressure of about 11 tons.

Synthesis of Graphene Oxide (GO)

GO was synthesized from natural graphite flakes following the modified Hummers method as has been discussed earlier.[32] The solid GO thus obtained was diluted to make its dispersion in deionized water (DIW) (5 mg/mL). This GO dispersion was dialyzed for 07 days for the removal of any remaining metal species. The 0.5 mg/mL of this dispersion was then exfoliated by sonication under ambient conditions for 30 min. The resulting homogeneous GO dispersion was stable for about six months and was used for performing further reaction(s).

Synthesis of N-doped Graphene Using Glycine (N-Gr)

Chemical reduction of GO to N-Gr was carried out by following the procedure reported earlier.[15] In brief, 52 mg of glycine (34.6 mM) was mixed with 20 ml of GO dispersion containing 10 mg of GO (0.5 mg/ml) under stirring and the pH of the resulting solution was adjusted to 10.5. The reaction mixture was heated on a circulating water bath for 3 h at 95 ^{0}C. The resultant black suspension was centrifuged and washed repeatedly from five to six times with DIW to remove any residual glycine as it is soluble in water.

Synthesis of N-doped graphene-Ag nanocomposites (N-GrAg)

For the synthesis of N-GrAg, 52 mg of glycine (34.6 mM) was mixed with 20 ml of GO dispersion containing 10 mg of GO (0.5 mg/ml) followed by the addition of 2 mg of $AgNO_3$ (0.59 x 10^{-3} M) under stirring and the pH of this solution was maintained at 10.5. The resulting reaction mixture was heated for 3 h on water bath at 95 ^{0}C. The completion of the reaction was monitored spectrophotometrically. The resultant black solution was centrifuged and washed with DIW from five to six times in order to remove any residual glycine.

The residual glycine in different washings for N-Gr and N-GrAg was estimated spectrophotometrically by using ninhydrin reagent[33] and was found to be absent even after two-three washings. The product thus obtained for these samples was re-dispersed in DIW and the pH of the solutions was maintained at 10.5.

Dalton Transactions Accepted Manuscript

For the comparison purposes, the control experiments were performed in the absence of reducing agent under the similar experimental conditions. In brief, 2 mg of $AgNO_3$ was mixed with 20 ml of GO dispersion containing 10 mg of GO (0.5 mg/ml) and the pH of the solution was maintained at 10.5 and heated for 3 h at 95 ^{0}C. This sample has been denoted as GO-Ag. Bare Ag NPs were also synthesized following the similar procedure as mentioned above in the absence of GO and it has been denoted as Gly-Ag.

Electrochemical Measurements

The GCE electrodes were polished sequentially by making slurry from alumina powder of size 1 µm followed by 0.5 and 0.03 µm using microcloth pad. The electrodes were rinsed thoroughly in an ultrasonic bath sequentially using DIW and ethanol for about 10 - 15 min, respectively. GCE electrodes were then dried under the flow of N_2. N-Gr and N-GrAg dispersions were prepared by suspending them in DMF (0.5 mg/mL) by ultrasonication for about 20-30 min. The homogeneously prepared solutions (6 µL) were drop-casted repeatedly in the aliquot of 2 µL after drying each time onto the surface of GCE electrode. The electrode surface was then allowed to dry overnight at room temperature. The loading mass on the working electrode was estimated to be about 0.042 mg/cm^2. All electrochemical measurements were performed at room temperature in 2 M KNO3 as an aqueous supporting electrolyte. The electrolyte was purged strongly with N_2 for about 5 min in order to remove any dissolved oxygen prior to performing electrochemical measurements.

SERS Measurements

The SERS activity of N-GrAg nanocomposites was measured by using (4-aminothiophenol) 4-ATP as a probe molecule. 50 µl of as synthesized N-GrAg (1 mg/ml) in ethanol was taken and it was mixed with the different concentrations of 4-ATP (1 x 10^{-3} – 5 x 10^{-8} M) to make the total volume of 200 µl. The resultant mixture was shaken for 1 h and was allowed to equilibrate for 3 h. In a control experiment, a typical concentration of 4-ATP (1 x 10^{-7} M) was adsorbed on N-Gr and bare Ag NPs by using the same procedure as was adopted for the adsorption of the 4-ATP on N-GrAg. An aliquot of about 10 µl of these solutions was applied on the glass plate and dried prior to recording the Raman spectra.

Results

Optical Studies

Optical absorption studies were used to monitor the formation of GO, N-doped graphene (N-Gr) and Ag coated N-Gr (N-GrAg) (Fig. 1). The optical absorption spectrum due to GO exhibit the peaks at 230 and 301 nm corresponds to π-π* and n-π* transitions, respectively (Fig. 1A-a). On the other hand, the reduction of GO using glycine in the absence of Ag^+ at pH 10.5 (N-Gr) shows a red shifted peak at 263 nm indicating the restoration of graphitic character (Fig. 1A-b). The N-GrAg nanocomposites were obtained by the reduction of GO in the presence of Ag^+ using glycine as a reducing agent at pH 10.5. For this process the amount of Ag^+ was optimized by varying its concentration and keeping the amounts of GO and glycine constant. At low concentration of Ag^+ containing the mass ratio of $AgNO_3$:GO (1:10), a peak at 259 nm in UV region and a broad peak at about 410 nm in visible region was observed (Fig. 1B-a). An increase in this mass ratio to 2:10 resulted in the red shifted peak at 262 nm associated with an increase in absorption in the visible region peaking at about 413 nm (Fig. 1B-b). A further increase in the mass ratios of $AgNO_3$:GO (3-9:10) caused the optical absorption in UV region to get gradually blue shifted associated with a reduction in its intensity. However, the peak at 413 nm becomes increasingly more intense with increasing Ag^+ (Fig. 1B-c to e). This clearly indicates that glycine is now involved mainly in reducing Ag^+ and reducing GO partially. This observation was also supported by the change in color from dark black to greenish at higher Ag^+ concentration (not shown). Thus, it suggest that $AgNO_3$:GO mass ratio of 2:10 is the optimum concentration for the simultaneous reduction of GO and Ag^+ which shows the development of peaks in UV region (262 nm) and visible region (413 nm). These bands can be assigned to the simultaneous reduction of GO to graphene and plasmonic absorption arising due to the formation of Ag NPs, respectively (Fig. 1C). The digital images of GO, N-Gr and N-GrAg exhibiting a change in color from yellowish brown to black in case of the later two samples are shown in the respective inset of Fig. 1A and C. The time duration for the heating of this reaction mixture was also optimized by recording the optical absorption spectra as a function of heating time (Fig. 1C-inset). With increased heating time from 1 – 3 h, the absorption in the UV and visible regions are observed to red shift from 255 to 262 nm and 402 to 413 nm, respectively associated with an increase in their absorbance. Any prolonged heating, did not result in any shift in the absorption maximum.

The stability of precursor GO, and as synthesized N-Gr and N-GrAg nanocomposites at the used pH of 10.5 was examined by performing the dynamic light scattering measurements in which the value of ζ-potentials were found to be -53.2, -40.7 and -49.6 mV, respectively (Fig. S1). These values of ζ-potentials suggest them to have fairly high stability.

XRD Studies

Fig. 2 presents the XRD patterns of GO, N-Gr and N-GrAg. The XRD pattern of GO shows peaks at 10.14 and 42.34° with the 'd' spacing of 0.872 and 0.214 nm, which corresponds to the reflection from (002) and (100) planes, respectively. This is very similar to the data reported previously for GO.[32] XRD pattern of N-Gr shows relatively broader peaks with high and low intensities at 2 theta values of 25.5 and 42.70° with the 'd' spacing of 0.349 and 0.212 nm corresponding to the reflection from (002) and (100) planes, respectively matching with the previous reports on N-doped graphene.[34] On the other hand, the N-GrAg shows a broad peak along with the several sharp peaks at 2 theta values of 24.55, 38.13, 44.27, 64.51, 77.46 and 81.68° analogous to the (002) plane of graphene and (111), (200), (220), (311) and (222) planes of Ag NPs matching to the face centered cubic (fcc) structure (JCPDS card no. 04-0783)

Dalton Transactions Accepted Manuscript

This journal is © The Royal Society of Chemistry 20xx

with the 'd' spacing values of 0.362, 0.236, 0.205, 0.144, 0.123 and 0.118 nm, respectively.[35] Using the Scherrer equation[36] the average crystallite size of Ag NPs was determined to be about 17 nm from the two highest intense reflection planes.

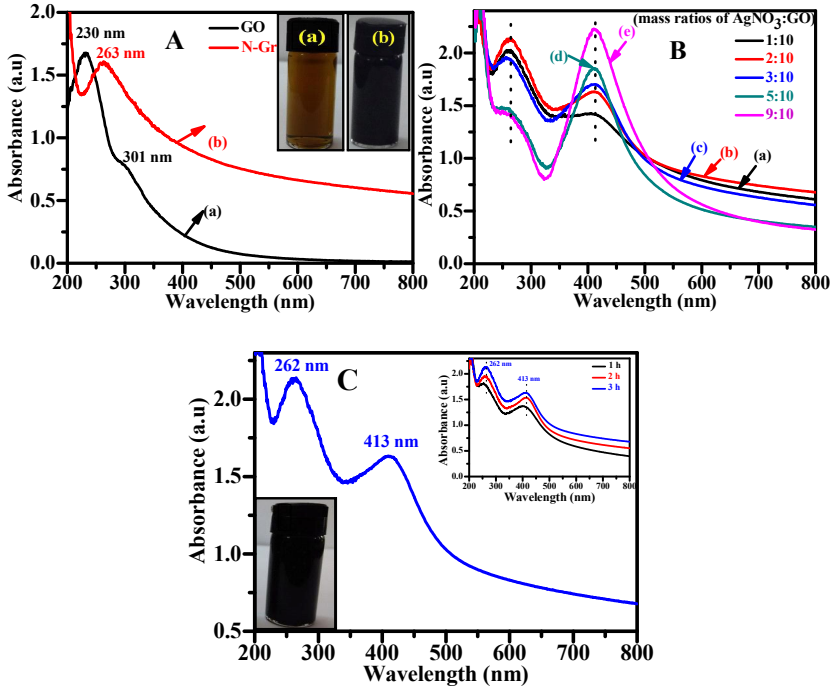

Fig. 1 Optical absorption spectra of GO (a) and N-Gr (b) along with their digital images in the inset- (panel A). Optical absorption spectra for the reduction of GO and Ag^{+} for the different mass ratios of $AgNO_3$:GO (1-9:10) – (panel B). Optical absorption spectra of N-GrAg and its digital image in the inset – (panel C). Optical absorption spectra of N-GrAg as a function of heating time – (panel C- inset).

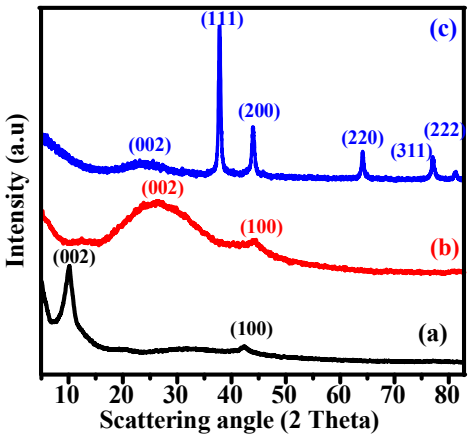

Fig. 2 XRD patterns of GO (a), N-Gr (b) and N-GrAg (c).

Raman Spectroscopy

Raman spectroscopy was used to study the electronic structures of GO, N-Gr and N-GrAg. Their spectral data have been summarized in Table S1. The Raman spectrum of GO is shown in Fig. S2. It exhibits typical D and G bands at 1354 and 1605 cm^{-1} similar to those observed previously[15] and its I_D/I_G ratio was worked out to be 0.89. The Raman spectrum of N-Gr also exhibited D and G bands at 1349 and 1604 cm^{-1}, respectively along with an additional D´ band at 1623 cm^{-1} (Fig. 3A-a) possibly arising due to the doping of N. Moreover, in this case the I_D/I_G ratio is increased to 1.00 as compared to that of GO (0.89) similar to those observed earlier for N- doped graphene.[15] The increase in the I_D/I_G ratio for N-Gr suggests the effective reduction of GO accounting for the increased number of smaller sp^2 domains.

The Raman spectrum of the optimized N-GrAg sample as was arrived by optical absorption spectroscopy for the mass ratio of 2:10 ($AgNO_3$:GO) was recorded in Fig. 3A-b. It shows that the peak intensities of D and G bands are enhanced by about 365 % as compared to that of N-Gr upon decoration with Ag NPs. It also exhibited the D´ band at 1623 cm^{-1}, suggesting the effective doping of N has taken place in N-GrAg similar to that of N-Gr (Fig. 3B). A further increase in the I_D/I_G ratio for this sample (1.03) suggests the increased defects formation on the surface of N-Gr upon the decoration by Ag NPs. This aspect was further probed by calculating the in – plane crystallite size (L_a in nm) which comes out be 20.18, 16.75 and 16.26 nm for GO, N-Gr and N-GrAg, respectively. The value of L_a follows the order: GO > N-Gr > N-GrAg supporting the increased defects formation upon doping of N and its further functionalization by Ag. These features suggest the effective reduction of GO to N-GrAg under these conditions, as has also been observed earlier for N-doped graphene decorated by Ag using other reducing agents.[37,25]

Dalton Transactions Accepted Manuscript

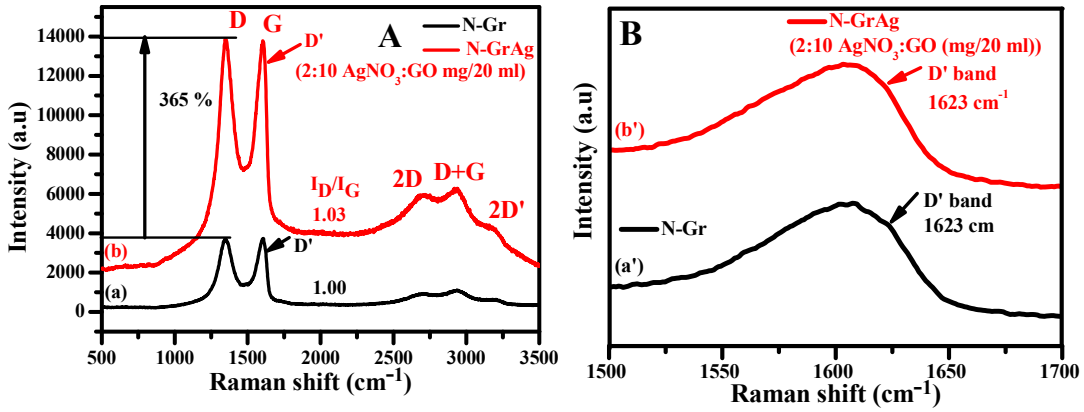

Fig. 3 Raman spectra of: N-Gr (a) and N-GrAg (b) – (panel A); expanded D' band of: N-Gr (a') and N-GrAg (b') in the range of 1500 – 1700 cm^{-1} – (panel C).

AFM Analysis

The surface topography of the precursor GO and the products, N-Gr, and N-GrAg, was examined by AFM and their 2-D images are shown in Fig. 4. The surface roughness of GO sheet along a particular line marked in its 2D image (Fig. 4a) was found to be 1.18 nm, which has been reported previously corresponding to single layer.[31] On the other hand, the average surface height of N-Gr sheet along a particular marked line as well as from several other locations on this sheet was computed to be 0.88 ± 0.15 nm (Fig. 4b), which is smaller than that of GO. This decrease in average surface height is attributed to the removal of functionalities from the surface of GO. It may be noted that the surface heights for GO and N-Gr were recorded at the locations, where the folding was not apparent.

The AFM image of N-GrAg shows that the entire N-Gr sheet is uniformly decorated by Ag NPs and the average particle size (size distribution) of Ag NPs over the entire graphene sheet was estimated to be 18 nm (10 – 32 nm) (Fig. 4c). For a typical case, the surface height along a particular line marked in Fig. 4c, where Ag NPs were present in a continuous array shows the average size of Ag NPs to be 16 nm (Fig. 4c'). Moreover, the nature of graphene sheet seems to be modified in N-GrAg upon the decoration of Ag NPs as its folding is not apparent unlike to the bare graphene sheet in N-Gr. It suggests that the binding of Ag NPs does not allow the folding of the graphene sheet.

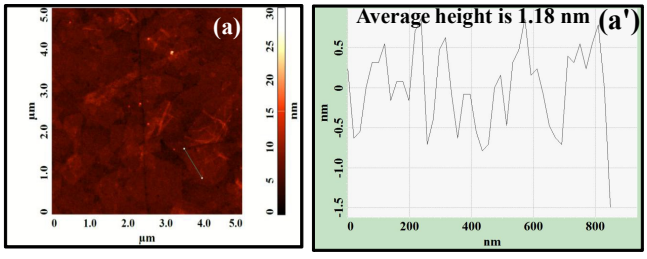

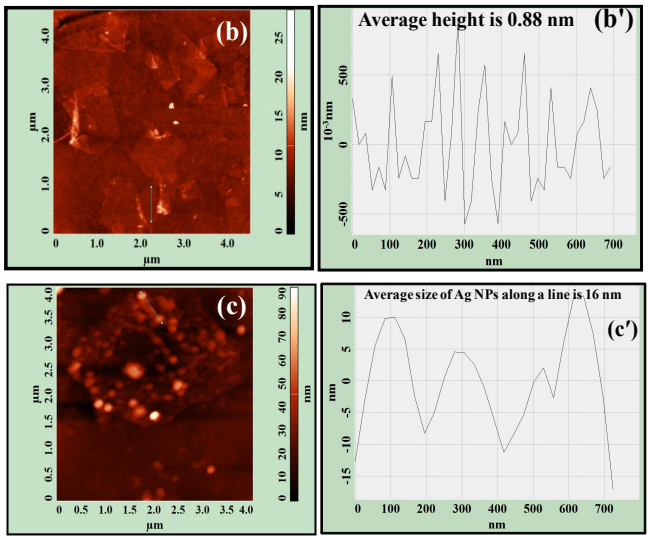

Fig. 4 AFM images and their height profile along a partcular line: GO (a and a'), N-Gr (b and b') and N-GrAg (c and c'), respectively.

FESEM Analysis

The morphologies of GO, N-Gr and N-GrAg were further examined by FESEM analysis (Fig. 5).The EDAX spectra of the FESEM images were recorded at the locations marked by (+) sign in red. FESEM image of GO indicates it to contain aggregated sheets consisting of C and O elements (Fig. 5a and a'). FESEM image of N-Gr exhibits relatively a very thin and crumpled sheet and its EDAX analysis shows the presence of N apart from C and O (Fig. 5b and b'). On the other hand, the FESEM image of N-GrAg exhibits fairly high density of spherical Ag NPs on the surface of N-Gr sheet (Fig. 5c). Its EDAX analysis shows the presence of C, N, O along with the presence of Ag in N-GrAg (Fig. 5c'). The elemental mapping of a portion of this sheet indicated by the red square in this image shows the homogeneous distribution of C, N, O along with Ag. These results clearly support the uniform distribution of Ag NPs on the graphene sheet in N-GrAg.

Dalton Transactions Accepted Manuscript

This journal is © The Royal Society of Chemistry 20xx

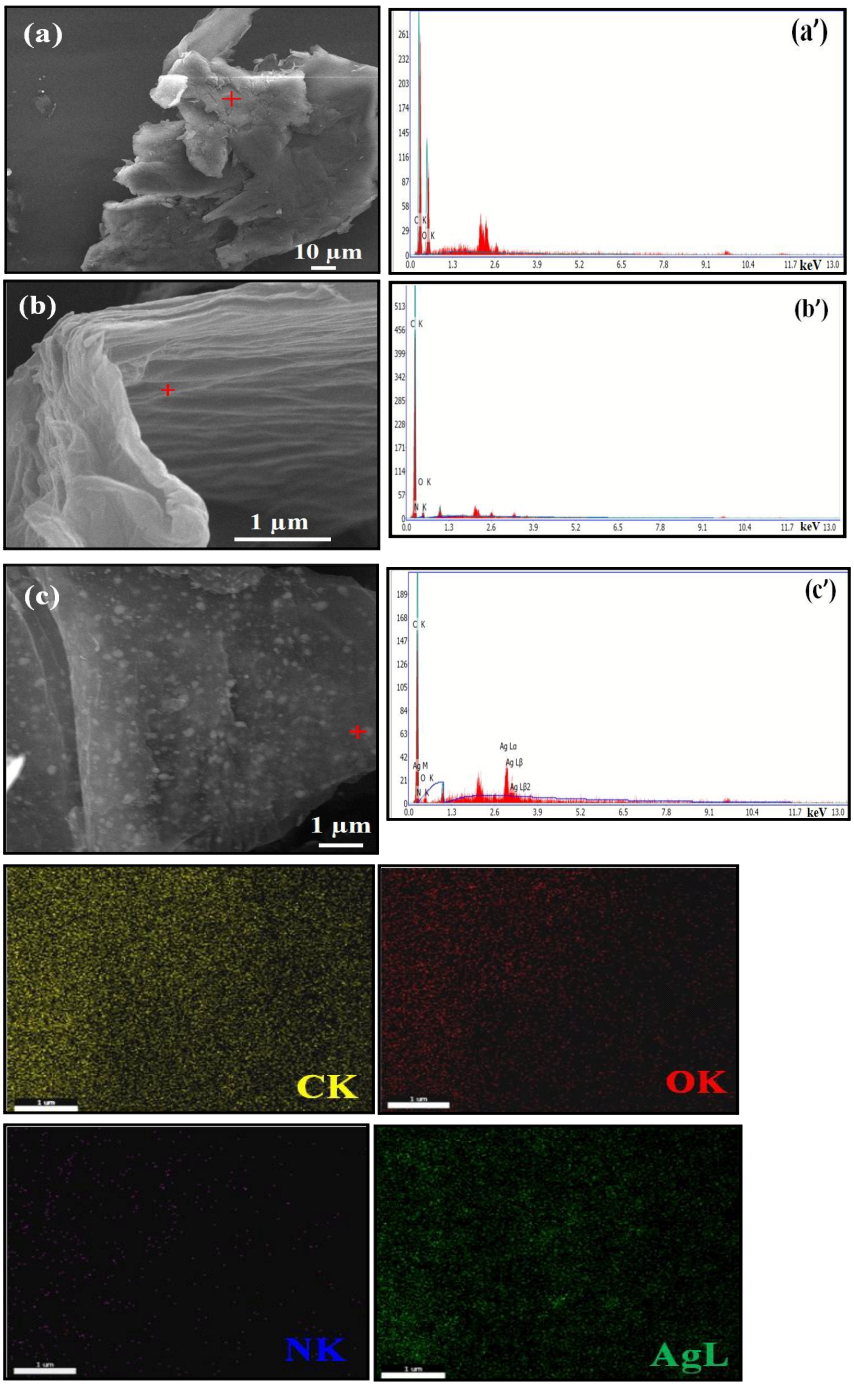

Fig. 5 FESEM and EDAX images of GO (a and a'), N-Gr (b and b') and N-GrAg (c and c'). Elemental mapping images of N-GrAg showing C, O, N and Ag elements.

TEM Analysis

TEM images of GO, N-Gr and N-GrAg along with their SAED patterns and EDAX analysis are shown in Fig. 6. TEM images of all these samples exhibit sheet-like structure (Fig. 6a, b and c). GO sheets appeared to be relatively thicker as compared to that of N-Gr (Fig. 6a). Whereas, N-Gr sheet shows wrinkles and folding at various locations (Fig. 6b). On the other hand, N-GrAg exhibits the surface of the sheet without folding and wrinkles, which is uniformly decorated with Ag NPs (Fig. 6c). The average particle size of Ag NPs (size distribution) on the surface of N-Gr sheet was estimated from various such images prepared at different times and found to be 17.5 nm (10 – 32 nm) (Fig. 6c'). SAED pattern of GO exhibits the ring pattern displaying polycrystallinity very similar to that reported previously[32] (Fig. 6a - inset). Whereas, the SAED pattern of N-Gr clearly shows it to be crystalline with six-fold symmetry (Fig.

Dalton Transactions Accepted Manuscript

6b - inset). On the other hand, the SAED pattern of N-GrAg also exhibits ring pattern with bright spots displaying polycrystallinity corresponding to the (111), (200), (220), (311), (222) and (420) planes matching to the fcc structure of Ag NPs (JCPDS file no. 04-0783) (Fig. 6c''). From HRTEM image of N-GrAg, the 'd' spacing was calculated to be 0.236 nm which matches to the most intense reflection from (111) plane matching to the fcc structure of Ag NPs (Fig. 6c'''). EDAX analysis of these samples clearly shows the presence of C and O in GO; C, O, and N in N-Gr and C, O, N and Ag in case of N-GrAg (Fig. S3a and b; Fig. 6c'''').

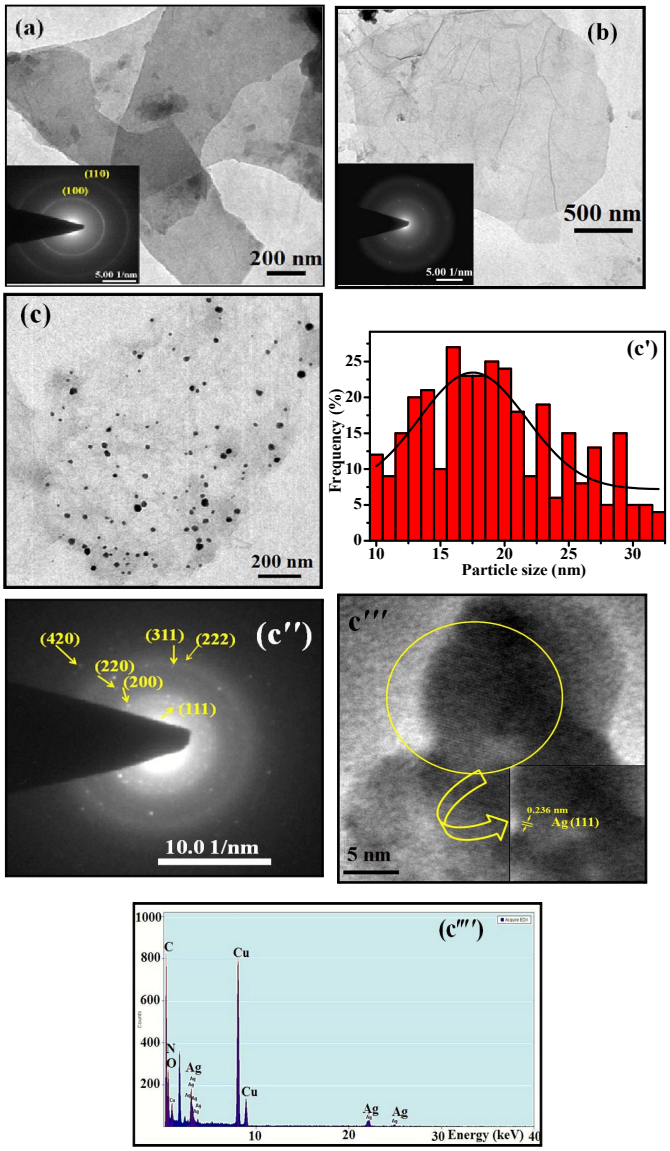

Fig. 6 TEM images of GO (a) and N-Gr (b) along with their SAED patterns in the inset. TEM micrograph, particle size distribution and SAED pattern of N-GrAg (c, c' and c''); HRTEM image of N-GrAg (c''') and its magnified image showing a 'd' spacing corresponding to Ag (111) plane (c'''- inset); EDAX analysis of N-GrAg (c'''').

BET Analysis

The decoration of Ag NPs on N-Gr in N-GrAg leads to the unfolding of graphene sheet and exhibited different morphologies, it was further probed by analyzing its BET surface area. From these measurements, the specific surface area of N-Gr and N-GrAg were estimated to be 360 and 523 m^2/g, respectively. As expected, the specific surface area of N-GrAg is about more than 1.4 times higher than that of N-Gr suggesting the immobilization of Ag on the surface of N-Gr preventing its aggregation. From DFT method the average pore diameter (pore size distribution) of N-Gr and N-GrAg were found to be: 1.66 nm (1.5 – 3.6 nm) and 1.58 nm (1.3 – 3.4 nm) suggesting them to be microporous, respectively (Fig. S4).

FTIR Spectroscopy

FTIR spectra of GO, N-Gr and N-GrAg are shown in Fig. 7. The various prominent vibrational bands (cm^{-1}) for GO were observed at 3435, 2925, 2853, 1730, 1629, 1382, 1221 and 1054, which have been assigned to –OH stretching, symmetrical and unsymmetrical -C-H stretching, C=O (carboxylic), C=C, C-OH (stretching/deformation), C-O-C (epoxy) and C-O (alkoxy) oxygen functionalities, respectively and matches to the previously reported data on GO.[38] The reduction of GO into N-Gr results in the reduction of intensity of vibrational band due to –OH stretching. It also results in the complete disappearance of the peaks due to C=O and C-O-C functionalities (panels A and B). However, the peaks due to C-O and C-OH become fairly weak and broad. Furthermore, a weaker and less intense bands due to –C-H stretching were observed as compared to that for GO, which might have occurred due to the doping of N as has also been noted previously.[39] The doping of N is further indicated by the appearance of a new broad peak in the vicinity of 1580 cm^{-1}, which is likely to arise from co-contribution of both aromatic C=C and –N-H bending. Apart to this, a weak and broad peak is also observed at 1340 cm^{-1}, which has been assigned to C-N stretching. The in-situ generation of Ag NPs on the surface of N-Gr (N-GrAg) does not bring any change in the vibrational spectrum of N-Gr, except that a broad peak due to C=C stretching, the band due to –N-H bending and C-N stretching are slightly shifted to lower wavenumber (cm^{-1}) from 1629 to 1621, 1580 to 1573, and 1340 to 1245 – 1280, respectively.

Solid-state ^{13}C NMR Spectroscopy

The reduction of GO and doping of N into N-Gr and N-GrAg were also examined by using solid-state ^{13}C MAS NMR spectroscopy (Fig. 8). The ^{13}C spectrum of GO exhibits various peaks at about 61, 70, 105, 115, 129, 167 and 190 ppm which have been assigned to epoxy (C-O-C), hydroxyl (C-OH), sp^2 carbon with graphitic structure in different environments, carboxylic (O-C=O) and ketonic carbon (C=O), respectively which is very similar to the previous reports.[31,40] Interestingly, in N-Gr sample, the functionalities like C-O-C, O=C-O and C=O are almost completely eliminated and the peak due to C-OH functionality is significantly reduced along with its broadening.

Dalton Transactions Accepted Manuscript

This journal is © The Royal Society of Chemistry 20xx

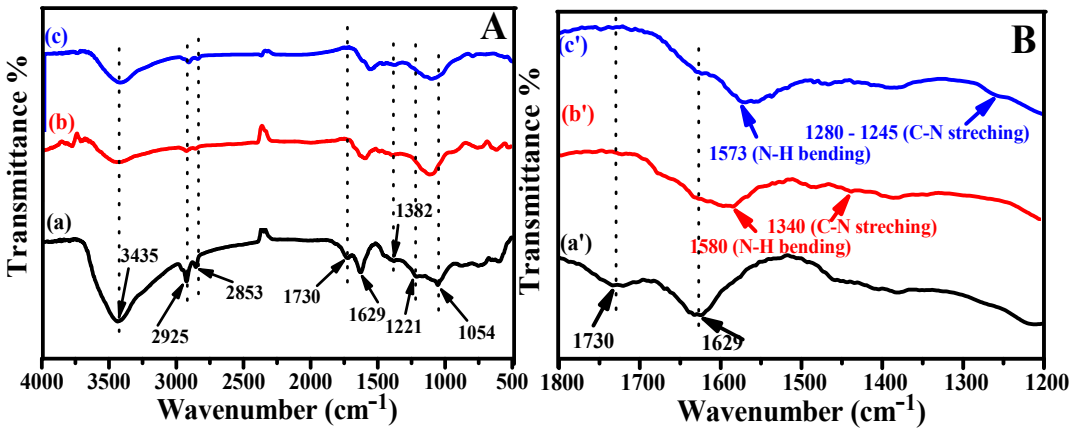

Fig. 7 FTIR spectra of: GO (a), N-Gr (b) and N-GrAg (c) – (panel A); expanded FTIR spectra of: GO (a′) N-Gr (b′) and N-GrAg (c′) in the 1800–1200 cm^{-1} range (panel B).

The graphitic sp^2 carbon peaks has now become more intense, broadened and up-shifted. It suggests an increase in the graphitic nature of the N-Gr as observed earlier.[41] The ^{13}C NMR spectrum of N-GrAg remains unchanged except that the sp^2 carbon peak has further shifted to upfield and broadened, which clearly indicates that the sp^2 character is further increased in N-GrAg. As a matter of fact a new peak was developed in both the samples (N-Gr and N-GrAg) at about 172 and 174 ppm, respectively which is attributed to the formation of imine (C=N) functionality as reported earlier.[42]

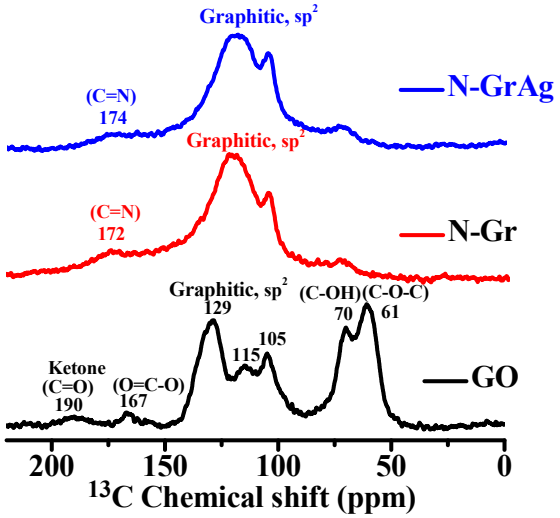

Fig. 8 Solid-state ^{13}C NMR of GO, N-Gr and N-GrAg.

XPS Measurement

The surface analysis of N-Gr and N-GrAg nanocomposites was performed by using XPS. The survey scans of these samples in the range of 200-800 eV are presented in Fig. 9A indicating the presence of C 1s, N 1s and O 1s in N-Gr; C 1s, N 1s, O 1s and Ag 3d in N-GrAg. The high resolution C 1s and N 1s spectra for N-Gr and C 1s, N 1s and Ag 3d for N-GrAg are shown in Fig. 9B-F. The C 1s spectrum of N-Gr is deconvoluted into three different components of carbon (eV) at 284.5, 285.6 and 288.2 corresponding to C-C/C=C (sp^3/sp^2 carbon), C-O/C-N (alcohol/epoxy/alkoxy/carbon singly bonded to nitrogen and C=O (carboxyl) groups, respectively (Fig. 9B). Interestingly, a new peak is observed in N-Gr at 285.6 eV which is slightly shifted to lower binding energy than to that of GO (286.0 eV)[31] (Fig. S5) and has been assigned to the C-O/C-N. However, it is difficult to isolate the presence of C-O/C-N at this binding energy as these binding energies are fairly close.[25] The N 1s spectrum of N-Gr has been deconvoluted into three components of N: pyridinic-N (397.9 eV), pyrolic-N (399.9 eV) and quaternary-N (402.0 eV) (Fig. 9C). It is apparent from the area under these peaks that the major component among these N moieties corresponded to the pyrolic-N. The high resolution C 1s spectrum of N-GrAg also exhibits three different components of carbon at (eV): 284.5, 285.7 and 288.0 eV very similar to that observed in N-Gr (Fig. 9D). N 1s spectrum of this sample also exhibited three different components of N: pyridinic-N (398.5 eV), pyrolic-N (400.0 eV) and quaternary-N (401.7 eV), but the binding energy corresponding to pyridinic and pyrolic-N were slightly shifted to higher energies as compared to that present in case of N-Gr (Fig. 9E). For this sample also the major component corresponded to the pyrolic-N. Ag 3d doublet spectrum for N-GrAg is shown in panel F. It shows two peaks at 368.4 and 374.4 eV which could be assigned to characteristic Ag 3d doublet corresponding to Ag $3d_{5/2}$ and Ag $3d_{3/2}$, respectively (Fig. 9F). These peaks are present at a slightly higher binding energies by about 0.5 eV as compared to that of bulk metallic Ag.[25] This shift to higher energies could be attributed to the binding of Ag to N-Gr. The elemental composition for N-GrAg shows C (80.3 %), N (1.91 %), O (17.4 %) and Ag (0.309 %). This clearly indicates the doping/effective functionalization of graphene sheets by N and their decoration by the Ag NPs.

Dalton Transactions Accepted Manuscript

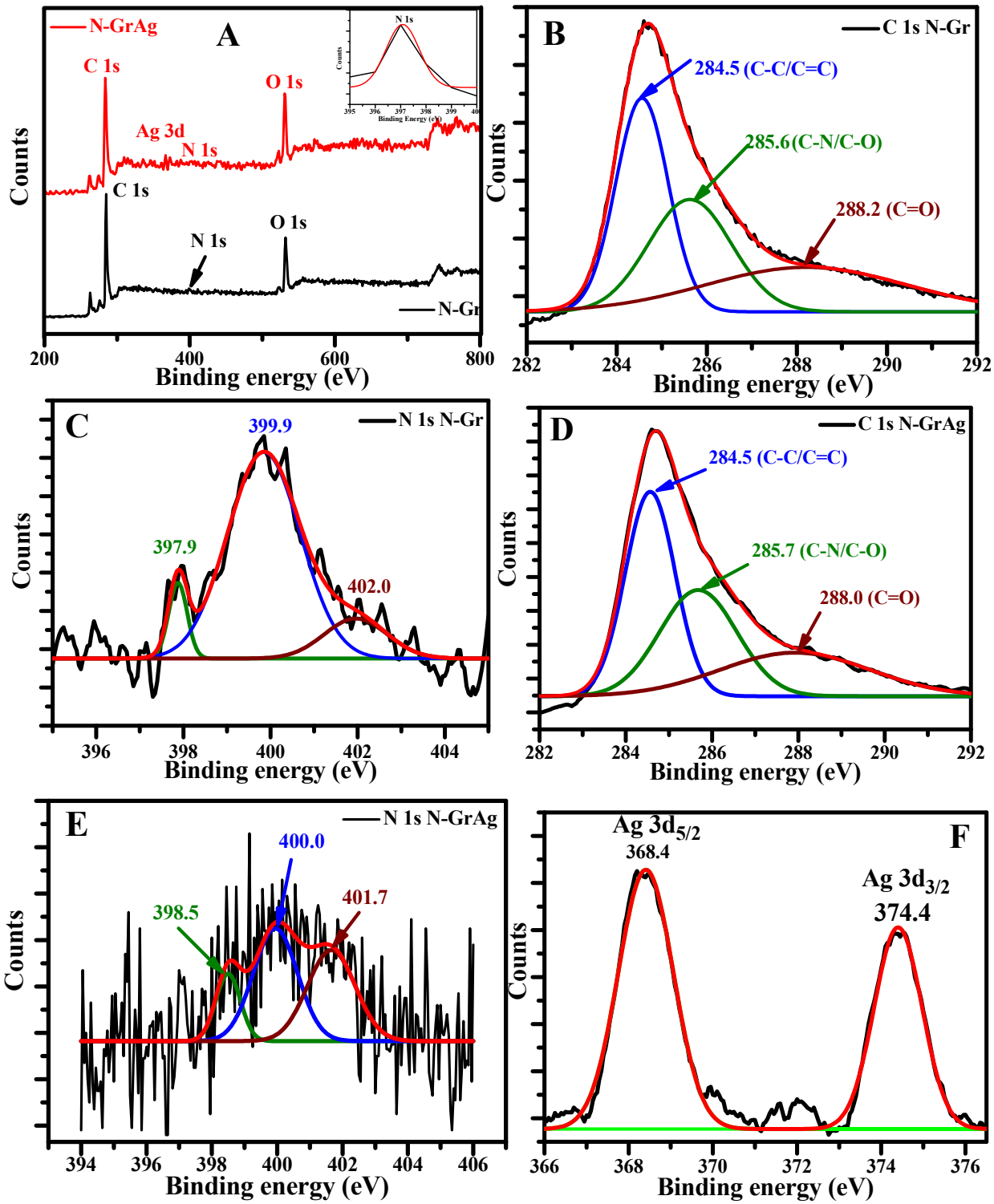

Fig. 9 XPS survey scans of: N-Gr (a) and N-GrAg (b), inset N 1s – (panel A); high resolution C 1s and N 1s spectra of N-Gr – (panels B and C); C 1s, N1s and Ag 3d spectra of N-GrAg - (panels D-F).

TGA Measurement

The thermal stability of the precursor GO and the products, N-Gr and N-GrAg, was examined by recording their TGA curves (Fig. 10). The TGA curve of GO exhibits 14% weight loss at about 100 ^{0}C, which is assigned to the removal of adsorbed water and the second major weight loss of 29 % occurred at about 195 ^{0}C and has been attributed to the decomposition of labile oxygen functionalities such as carboxylic, anhydride and

Dalton Transactions Accepted Manuscript

This journal is © The Royal Society of Chemistry 20xx

lactone groups as observed in previous report.[15] Whereas, in case of N-Gr there is about 8 % of weight loss at around 100 ^{0}C and only 14 % of weight loss occurs at about 200 ^{0}C. The third slow but steady major loss started from about 430 ^{0}C and, which was followed by a steep loss in weight up to 540 ^{0}C amounting to be about 90%. Thereafter, it becomes almost constant. The weight loss in this range corresponds to the removal of stable oxygen functionalities (phenols and carbonyl). Whereas, in case of N-GrAg the weight loss at 100 and 200 ^{0}C are reduced to about 6 and 10 %, respectively. In this case the third major weight loss started at about 430 ^{0}C and unlike to that of N-Gr, occurred up to 500 ^{0}C only, which has been estimated to be about 68%. These nanocomposites were found to be fairly stable up to 800 ^{0}C. It clearly shows that the as synthesized nanocomposites are apparently more stable as compared to those of GO and N-Gr.

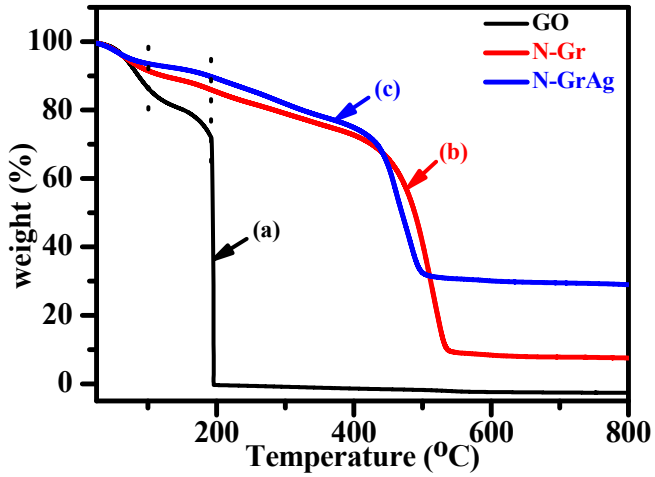

Fig. 10 TGA curves of GO (a), N-Gr (b) and N-GrAg (c).

Current-Voltage (I-V) Measurements

The I-V curves of N-Gr and N-GrAg are presented in Fig. 11. These plots show linearity over the entire voltage range (-1 to + 1 V) suggesting them to follow the ohmic behavior. In case of N-Gr, a drastic increase in conductivity (11.4 S/cm) is observed as compared to that of GO (2.7 x 10^{-4} S/cm).[31] This value is about four orders of magnitude higher as compared to that of GO and could be attributed to the removal of the oxygen functionalities from its surface. The decoration of Ag NPs on the surface of N-Gr sheet (N-GrAg) further enhances its conductivity to 25.9 S/cm which is more than two-fold higher with that of N-Gr. The increase in conductivity for N-GrAg possibly arises due to the increased delocalization of the π-electrons in the presence of Ag on N-Gr. It also prevents the aggregation of graphene sheet in N-GrAg as is evident from its AFM/TEM images (Fig. 4 and 6), which might have contributed to its higher conductivity.

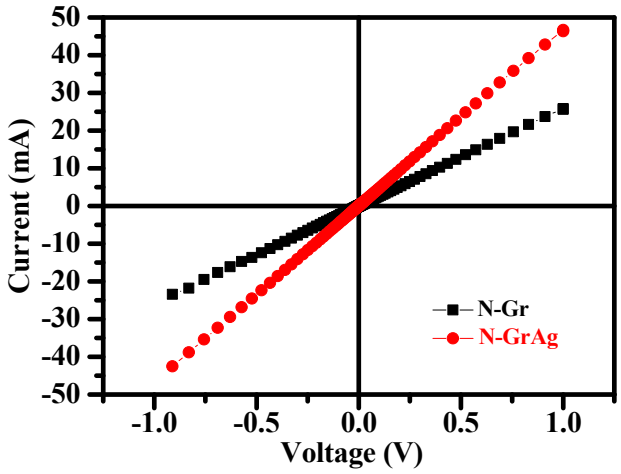

Fig. 11 I-V curves of N-Gr (black) and N-GrAg (red).

Electrochemical Measurements

The electrochemical behavior of N-Gr and N-GrAg was analyzed by using cyclic voltammetry (CV) in 2 M KNO_3 as an aqueous supporting electrolyte (Fig. 12A). The CV measurements were recorded in the potential window of 0 – 0.8 V at a scan rate of 100 mV/s. N-Gr exhibits almost rectangular shape arising from electric double layer capacitance (EDLC) along with the contribution from pseudo-capacitance developed due to the different moieties of N (pyridinc/pyrolic/quaternary). Whereas, in the case of N-GrAg a pair of fairly well separated redox peaks were observed at 0.45 and 0.29 V corresponding to the anodic and cathodic peaks, respectively. A careful examination of this curve indicates that the anodic peak is relatively sharper than that of cathodic peak. Moreover, these peaks are broad and asymmetrical which might be arising because of the existence of the multiple redox involving the interaction of Ag and N-Gr functionalities. From these curves the specific capacitance (C_s in F/g) values for N-Gr and N-GrAg were calculated to be 130 and 346, respectively. The C_s value for N-GrAg (346 F/g) is more than 2.6 times higher as compared to that of N-Gr (130 F/g). Moreover, the observed vale of C_s for N-GrAg in the present case is much higher to that reported earlier for Ag/RGO (220 F/g).[24]

Electrochemical impedance spectroscopy (EIS) was performed to further analyze the resistance characteristic of N-Gr and N-GrAg (Fig. 12B). The Nyquist plots (imaginary (Z'') *Vs* real (Z') component) for both the samples did not show any semi-circle in the high frequency region indicating the low resistance. However, a careful examination of these curves reveals that the N-Gr exhibits slightly higher resistance as compared to that of N-GrAg in the high frequency range. The low frequency region for both the samples exhibit linear curve variation with a steeper slope for N-GrAg which suggest the faster ion transport diffusion for N-GrAg. Thus, the curve for N-GrAg displays good capacitive behavior in both the frequency regions.

Dalton Transactions Accepted Manuscript

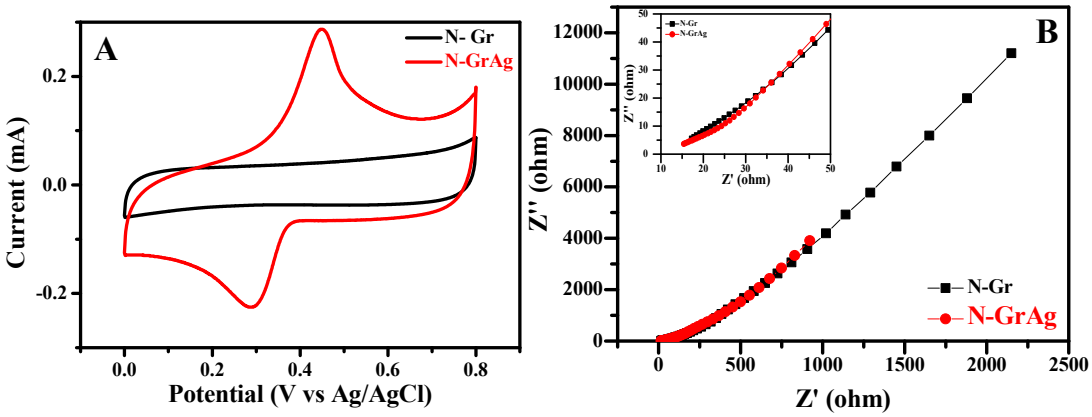

Fig. 12 CV curves of N-Gr and N-GrAg at a scan rate of 100 mV/s in 2 M KNO_3 as an aqueous supporting electrolyte – (panel A). Nyquist plots of N-Gr and N-GrAg in the frequency range of 0.1 Hz – 10 kHz at an amplitude of 10 mV – (panel B); expanded high frequency region of N-Gr and N-GrAg (panel B - inset).

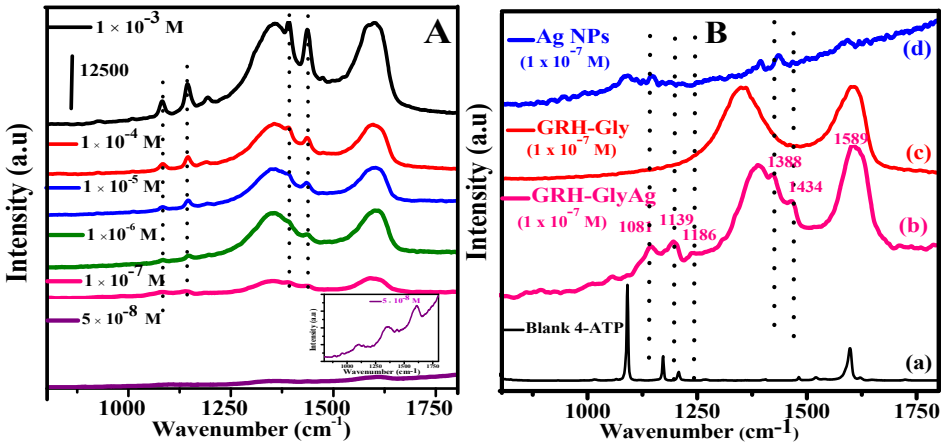

Fig. 13 SERS spectra of 4-ATP adsorbed on N-GrAg nanocomposites at its various concentrations (1 x 10^{-3} – 5 x 10^{-8} M) – (panel A). Raman spectrum of solid neat 4-ATP (a) and SERS spectra of 4-ATP (1 x 10^{-7} M) adsorbed on N-Gr (b), bare Ag NPs (c) and N-GrAg (d) - (panel B).

SERS Measurements

The SERS activity of N-GrAg nanocomposites was evaluated by using 4-aminothiophenol (4-ATP) as a probe molecule (Fig. 13). The SERS spectra of 4-ATP adsorbed on N-GrAg nanocomposites at its various concentrations (1 x 10^{-3} – 5 x 10^{-8} M) have been shown in Fig. 13A. The Raman spectrum of solid 4-ATP exhibits several distinctive (strong and medium) bands (cm^{-1}) at: 1091, 1172, 1598, 1120, 1208 and 1482 (Fig. 13B-a). For a typical 4-ATP concentration (1 x 10^{-7} M) adsorbed on N-GrAg, these bands (cm^{-1}) are observed at about 1081, 1139, 1186, 1388, 1589 and 1434 (Fig. 13B-b) in the present work, which are very similar to those observed earlier for Ag NPs-graphene nanocomposites.[29] A comparison of the Raman spectrum of blank 4-ATP (Fig. 13B-a) with that obtained after its adsorption on N-GrAg (Fig. 13B-b) clearly reveals the distinctive shifts in the frequencies of 4-ATP (cm^{-1}) from 1091 to 1081 and 1598 to ~1589 and have been assigned to the formation of carbon-sulphur (C-S) bond and Ag-S bond between Ag NPs and –SH group of 4-ATP, respectively.[29] These shifts are indicative of the interaction of 4-ATP with Ag NPs present on the surface of N-Gr. In control experiments, the SERS activity of N-Gr and bare Ag NPs for 4-ATP adsorbed on their surface at its typical concentration of 1 x 10^{-7} M have been shown in Fig. 13B-c and d. For the 4-ATP (1 x 10^{-7} M) adsorbed on the N-Gr sheets and bare Ag NPs, the intensities of the bands were, however, very weak. The much higher intensity of Raman bands in case of N-GrAg clearly reveals its excellent SERS activity.

Discussion

The reduction of GO and GO/Ag^+ to N-Gr and N-GrAg, respectively by employing glycine as a reducing agent was indicated by the optical absorption spectroscopy (Fig. 1A and B). In the reaction mixture containing GO, glycine and Ag^+, there would be the competition between GO and Ag^+ for glycine along with the possibility of direct reaction between GO and Ag^+ as has been reported earlier.[26] The formation of N-GrAg was monitored by following the reduction of GO/Ag^+ as a function of the concentration of Ag^+ (Fig. 1B). At low concentration of Ag^+ containing Ag^+:GO mass ratio of 1:10, a part of GO remains unreacted as was revealed by optical

Dalton Transactions Accepted Manuscript

This journal is © The Royal Society of Chemistry 20xx

spectroscopy (Fig. 1B-a), whereas at a little higher concentration of Ag^+ having 2:10 mass ratio of Ag^+:GO, the reduction of GO was observed to be the maximum (Fig. 1B-b). A further increase in the concentrations of Ag^+ containing varied mass ratio of Ag^+:GO (3-9:10) possibly results in the reduction of Ag^+ at a much faster rate rather than accomplishing the reduction of GO, which became evident by the increasing strong plasmonic absorption of Ag NPs (Fig. 1B - c to e). Thus, at varied mass ratios of Ag^+:GO, the resultant optical absorption spectra arises due to the formation of graphene, Ag NPs and unreacted GO if any. In control experiments, the reaction between glycine and Ag^+ (Gly-Ag) and GO and Ag^+ (GO-Ag) in the absence of glycine were performed at 95 ^{0}C at pH 10.5 for 3 h. For Gly-Ag sample the appearance of plasmonic band at about 417 nm is attributed to the formation of Ag NPs (Fig. S6a). In case of GO-Ag, the optical absorption spectrum exhibited a broad absorption peak in the range of 230-260 nm peaking at 247 nm along with a plasmonic band at around 407 nm (Fig. S6b). It could be understood in terms of the partial reduction of GO under alkaline conditions[43] and formation of Ag NPs, respectively. Raman spectroscopy shows an increase in the I_D/I_G ratio for GO-Ag to 0.97 as compared to that of GO (0.89) (Fig. S7), which clearly suggests the production of more disordered state for GO-Ag nanocomposites and is assigned to the chemical interaction between GO and Ag NPs.[44] The XRD data for GO-Ag however, shows that a part of Ag^+ remains unreacted under these conditions and corresponds to Ag_2O (Fig. S8). The IR spectroscopy for GO-Ag showed the presence of relatively strong C=O stretching frequency, as is observed in IR spectrum of GO alone (Fig. S9). These features are quite different to those observed in the present system, i.e. for N-Gr/ N-Gr-Ag. Thus, ruled out the contribution of Gly-Ag and GO-Ag in the present system.

The effective reduction of GO by glycine to produce N-Gr (Fig. 2b) and *in situ* generation of Ag NPs on the surface of N-Gr was also evident by XRD pattern of N-GrAg (Fig. 2c). It exhibited Ag to be present in fcc structure, which was also revealed by its SAED analysis (Fig. 6c''). The I_D/I_G ratio in the Raman spectra followed the order: GO (0.89) < N-Gr (1.00) < N-GrAg (1.03) (Fig. S2 and 3). It suggested an increase in the number of smaller sp^2 domains for both N-Gr and N-GrAg, as was also supported by the decrease in-plane crystallite size, which followed the order: GO > N-Gr > N-GrAg. The appearance of D' band for the later two samples is indicative of the creation of additional defects due to the doping of N and functionalization by Ag NPs. The decoration of Ag NPs in N-Gr (N-GrAg) was also suggested by the enhancement in the intensities of D and G bands (Fig. 3A).

The morphologies of N-Gr and N-GrAg were examined by AFM, FESEM and TEM analysis (Fig. 4-6) which showed the thin and crumpled sheet for the former and relatively unfolded sheet for N-GrAg, the surface of which is homogeneously decorated with Ag NPs with an average particle size of 17.5 nm (Fig. 6). The size of Ag NPs was also supported by XRD analysis (Fig. 2).

In XRD pattern of N-GrAg a weak and broad peak corresponding to the (002) reflection with slightly increased 'd' spacing value (0.362 nm) as compared to that of N-Gr (0.349 nm) was observed. This is explained due to the weak interaction of Ag NPs produced on its surface through different nitrogen moieties generated upon doping of N (Fig. 2), resulting into the weakening and broadening of (002) plane of N-Gr.[36] The doping of N in both N-Gr and N-GrAg is also indicated by IR spectroscopy which showed the appearance of new peaks due to C-N stretching and N-H bending (Fig. 7). These peaks were shifted slightly to lower wavenumber(s) in N-GrAg to that of N-Gr, which is understood due to the binding of N with Ag NPs. The doping of N in N-Gr and N-GrAg is also examined by the ^{13}C solid-state NMR spectra, where the appearance of new broad peaks was noted at about 172 and 174 ppm, respectively corresponding to the formation of C=N bond (Fig. 8).

The formation of C-N bond was further corroborated by XPS analysis of N-Gr and N-GrAg, which exhibited the new bands at 285.6 and 285.7 eV, respectively in their C 1s spectra (Fig. 9B and D). The N 1s spectrum of N-Gr shows three different components of N at 397.9, 399.9 and 402.0 eV (Fig. 9C) corresponding to pyridinic, pyrrolic and quaternary-N which are shifted to 398.5, 400.0 and 401.7 eV, respectively in case of N 1s spectrum of N-GrAg (Fig. 9E). The shift of these peaks could be attributed to the binding of Ag NPs with different N moieties. The enhanced stability of N-GrAg nanocomposites revealed by TGA analysis also suggested the interaction of Ag NPs with N of graphene as well as their supramolecular interactions with π bonds of the graphene. These observations are in line with the IR data (Fig. 7). These interactions are also manifested by the change in morphology of N-GrAg as compared to that of N-Gr, which shows relatively much less folding of sheet upon decorating its surface with Ag NPs.

Based on the different interactions observed by XRD, IR, ^{13}C-NMR and XPS and discussed above, the formation of N-doped graphene sheet decorated with Ag NPs is presented in scheme 1.

The fairly high conductivity of N-Gr (11.4 S/cm) as compared to that of GO (2.7×10^{-4} S/cm) can be appreciated due to the effective reduction of GO and its simultaneous functionalization with N (Fig. 11). A further increase in the conductivity of N-Gr (11.4 S/cm) upon decorating its surface by Ag NPs in N-GrAg (25.9 S/cm) can be attributed to the presence of conducting Ag NPs and its increased surface area (523 m^2/g), as is also revealed by a change in its morphology observed by AFM, FESEM and TEM analyses (Fig. 4-6), than to that of N-Gr (360 m^2/g). A comparison of the value of conductivity for N-GrAg (25.9 S/cm) observed in the present work is 150 times higher to that reported previously (0.1667 S/cm) for reduced graphene oxide decorated with Ag NPs (Ag-rGO) by using electron beam radiation (350 kGy irradiation)[45] and also more than two fold higher to that of N-Gr (11.4 S/cm). It clearly indicates the importance of functionalization by N as well as incorporation of Ag in enhancing the conductivity.

Dalton Transactions Accepted Manuscript

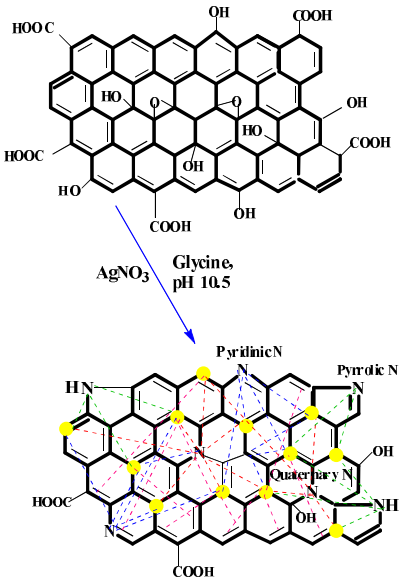

Scheme 1: Scheme for the formation of N-GrAg depicting the interaction of Ag NPs with different domains of N and π bond containing moieties present on the surface of N-Gr.

The high value of specific capacitance (C_s) observed in the present case for N-GrAg (346 F/g) than to that of N-Gr (130 F/g) (Fig. 12A) is attributed to the high electrical conductivity (25.9 S/cm), high surface area (523 m^2/g) and prevention of the aggregation of N-Gr due to the presence of Ag NPs on its surface. The unfolding of graphene is also expected to increase the active electrochemical surface area of N-GrAg which would have contributed to the high conductivity and high C_s. This observation is also supported by the EIS measurements where N-GrAg exhibited less resistance in both low and high frequency region as compared to N-Gr. Both of these studies suggest the better electrochemical behaviour of N-GrAg (Fig. 12B).

The interaction(s) of Ag through doped N moieties arrived by IR, ^{13}C NMR and XPS (Fig. 7-9) is also clearly evidenced by SERS measurements (Fig. 13). Where, an enhancement in the intensity of D and G bands in the Raman spectrum was observed by about 3.5 times in N-GrAg to that of N-Gr (Fig. 3A). SERS effect has been generally argued to occur through either electromagnetic (EM) or chemical (CM) enhancement mechanisms.[20,46] The excitation of localized surface plasmons in EM results in enormous enhancement of the Raman signal (10^{12}), whereas the CM enhancement has been considered to arise through the formation of charge transfer (CT) complexes between excited Ag and the SERS substrate resulting in relatively lower enhancement (10^1 - 10^2). Therefore, in N-GrAg, the observed enhancement of Raman signal by about 3-4 times to that of N-Gr, has been considered to arise through chemical interaction between Ag and N-Gr. It might have been contributed by the change in polarizibility occurring due to the charge-transfer interaction between the pyridine/pyridinic moieties of N-Gr and Ag NPs because of Ag having relatively low electronegativity than to that of nitrogen (Fig. 9).

The SERS activity of N-GrAg was further investigated by using 4-ATP as a probe molecule. The observed SERS activity of as synthesized nanocomposites containing the moderate average size (size distribution) of Ag NPs 17.5 nm (10-32 nm), demonstrated the fairly high detection limit for 4-ATP (5 x 10^{-8} M) and is very similar to that of Ag/rGO nanocomposites containing Ag NPs having the size in the range of 21.4 ± 10.5 nm, prepared by using arginine as a reducing agent.[28] The interaction of Ag in N-GrAg through –SH group of 4-ATP allowed its detection at fairly low concentration. However, in this work, extremely high concentration of $AgNO_3$ (100 mM) was employed[28] which is more than two orders of magnitude lower as compared to that used in the present work (0.59 mM). It thus makes the present system environmentally benign. These and some other important features of the previously reported similar systems have been summarized in Table 1. In fact the SERS activity in the present case could further be improved significantly by using Ag NPs of bigger size.[28] The enhanced electrical conductivity, surface area, specific capacitance and SERS of as synthesized nanocomposites suggest their potential for multifunctional applications.

Table 1: A comparison of synthetic details and some other important features of previously reported amino acid mediated synthesis of N-doped graphene-Ag nanocomposites.

Reducing Agent(s) (its concentration in mM)	**[Ag^+] (mM)/ Mass ratio (GO:amino acid:$AgNO_3$)**	**Ag (wt %)**	**Method; Temperature; Time**	**Size (size distribution) of Ag NPs**	**Surface area (m^2/g)**	**Electrical conductivity (S/cm)**	**Detection limit (nM) by SERS**	**Ref.**
Glycine (34.6)	0.59 /1:5.2:0.2	0.3 (surface at. %)	Thermal; 95 ^{0}C; 3 h	17.5 (10-32 nm)	523	25.9	50	**This work**
Glycine	-/1:2:2	-	Thermal; Temperature increased gradually from room temperature to 500 ^{0}C and maintained for 2 h	15-20 nm	Not Reported	Not Reported	Not Reported	27
Arginine (38.3)	100/1:13.3:33.8	69.6	Microwave (4 Cycles); (2.45 GHz, 900 W); 600 s (50 s 'on' and 10 s	21.4 ± 10.5 nm	Not Reported	Not Reported	10	28

Dalton Transactions Accepted Manuscript

This journal is © The Royal Society of Chemistry 20xx

			'off' for three times in each cycle)					

Conclusions

In summary, we have developed a one-pot method to synthesize N-doped graphene-Ag nanocomposites employing environmental benign reducing agent in aqueous medium under mild conditions. The in-situ generation of Ag NPs on the surface of N-Gr sheet prevents its aggregation through supramolecular interactions of Ag NPs with different domains of N and π bond containing moieties. These nanocomposites also demonstrated its potential for SERS for the detection of 4-ATP at a 50 nM. Thus, the as synthesized nanocomposites employing green precursors using relatively low temperature (95 °C) as compared to those used in previous studies having high surface area, conductivity, specific capacitance and SERS activity suggest it to be promising material for multifunctional applications.

Acknowledgements

Mahima Khandelwal is thankful to MHRD, New Delhi for the award of SRF. Thanks are also due to Head, IIC, IIT Roorkee, Roorkee for providing the facilities of FE-SEM, TEM and AFM.

References

1 V. Georgakilas, J.A. Perman, J. Tucek and R. Zboril, Chem. Rev., 2015, 115, 4744.
2 D.A.C. Brownson, D.K. Kampouris and C.E. Banks, Chem. Soc. Rev., 2012, 41, 6944.
3 X. Wang, G. Sun, P. Routh, D.-H. Kim, W. Huang and P. Chen, Chem. Soc. Rev., 2014, 43, 7067.
4 R.T. Lv and M. Terrones, Mater. Lett., 2012, 78, 209.
5 K. Fujisawa, , R. Cruz-Silva, K.-S. Yang, Y.A. Kim, T. Hayashi, M. Endo, M. Terrones, M.S. Dresselhaus, J. Mater. Chem. A, 2014, 2, 9532.
6 H. Wang, T. Maiyalagan and X. Wang, *ACS Catal*., 2012, **2**, 781.
7 R. Lv, Q. Li, A.R. Botello-Méndez, T. Hayashi, B. Wang, A. Berkdemir, Q. Hao, A.N. Elías, R. Cruz-Silva, H.R. Gutiérrez, Y.A. Kim, H. Muramatsu, J. Zhu, M. Endo, H. Terrones, J.-C. Charlier, M. Pan and M. Terrones, *Sci. Rep.*, 2012, **2**, 586.
8 Y. Qiu, X. Zhang and S. Yang, *Phys. Chem. Chem. Phys*., 2011, **13**, 12554.
9 X. Xu, L. Pan, Y. Liu, T. Lu and Z. Sun, *J. Colloid Interface Sci.*, 2015, **445**, 143.
10 S. Stankovich, D.A. Dikin, R.D. Piner, K.A. Kohlhaas, A. Kleinhammes, Y. Jia, Y. Wu, S.T. Nguyen and R.S. Ruoff, *Carbon*, 2007, **45**, 1558.
11 D. Long, W. Li, L. Ling, J. Miyawaki, I. Mochida and S.-H. Yoon, *Langmuir*, 2010, **26**, 16096.
12 J.W. Lee, J.M. Ko and J.-D. Kim, *Electrochim. Acta*, 2012, **85**, 459.
13 Y. Zhang, K. Fugane, T. Mori, L. Niu and J. Ye, *J. Mater. Chem*., 2012, **22**, 6575.
14 Y. Chang, G. Han, J. Yuan, D. Fu, F. Liu and S. Li, *J. Power Sources*, 2013, **238**, 492.
15 A. Kumar and M. Khandelwal, *New. J. Chem*., 2014, **38**, 3457.
16 S. Bose, T. Kulia, A.K. Mishra, N.M. Kim and J.H. Lee, *J. Mater. Chem*., 2012, **22**, 9696.
17 C. Zhang, M. Chen, X. Xu, L. Zhang, L. Zhang, F. Xia, X. Li, Y. Liu, W. Hu, J. Gao, *Nanotechnology*, 2014, **25**, 135707.
18 T. Wang, L. Wang, D. Wu, W. Xia, H. Zhao and D. Jia, *J. Mater. Chem. A*, 2014, **2**, 8352.
19 C. Tan, X. Huang and H. Zhang, *Mater. Today*, 2013, **16**, 29.
20 M. Khan, M.N. Tahir, S.F. Adil, H.U. Khan, M.R.H. Siddiqui, A.A. Al-warthan and W. Tremel, *J. Mater. Chem. A*, 2015, **3**, 18753.
21 K. Kim, K. Hong, B. Koo, I. Lee and J.-L. Lee, *Appl. Phys. Lett*., 2013, **102**, 081118.
22 T. Wu, S. Liu, Y. Luo, W. Lu, L. Wang and X. Sun, Nanoscale, 2011, **3**, 2142.
23 S. Liu, J. Tian, L. Wang and X. Sun, Carbon, 2011, **49**, 3158.
24 L. Zheng, G. Zhang, M. Zhang, S. Guo and Z.-H. Liu, *J. Power Sources*, 2012, **201**, 376.
25 B.K. Barman and K.K. Nanda, *RSC Adv*., 2014, **4**, 44146.
26 R. Pasricha, S. Gupta and A.K. Srivastava, *Small*, 2009, **20**, 2253.
27 S. Mayavan, J.-B. Sim and S.M. Choi, *Carbon*, 2012, **50**, 5148.
28 K.-C. Hsu and D.-H. Chen, *Nanoscale Res. Lett.*, 2014, **9**, 193.
29 Y. Zhang, S. Liu, L. Wang, X. Qin, J. Tian, W. Lu, G. Chang and X. Sun, *RSC Adv*., 2012, **2**, 538.
30 M.J. Fernández-Merino, S. Villar-Rodil, J.I. Pardes, P. Solís-Fernández, L. Guardia, R. Garćia; A. Martínez-Alonso and J.M.D. Tascón, *Carbon*, 2013, **63**, 30.
31 M. Khandelwal and A. Kumar, *J. Mater. Chem. A*, 2015, **3**, 22975.
32 A. Kumar and M. Khandelwal, *J. Mater. Chem. A*, 2014, **2**, 20345.
33 S. Moore and W. H. Stein, *J. Biol. Chem*., 1948, **176**, 367.
34 V. Sahu, S. Grover, B. Tulachan, M. Sharma, G. Srivastva, M. Roy, M. Saxena, N. Sethy, K. Bhargava, D. Philip, H. Kim, G. Singh, S.K. Singh, M. Das and R.K. Sharma, *Electrochim. Acta* 2015, **160**, 244.
35 K.H. Leong, L.C. Sim, D. Bahnemann, M. Jang, S. Ibrahim and P. Saravanan, *APL Mat*., 2015, **3**, 104503.
36 A.L. Patterson, *Phys. Rev*., 1939, **56**, 978.
37 Y. Tian, F. Wang, Y. Liu, F. Pang and X. Zhang, *Electrochim. Acta*, 2014, **146**, 646.
38 Y. Feng, N. Feng and G. Du, *RSC Adv*., 2013, **3**, 21466.
39 J.H. Kaufman, S. Metin and D.D. Saperstein, *Phys. Rev. B.*, 1989, **39**, 13053.
40 W. Gao, L.B. Alemany, L. Ci and P.M. Ajayan, *Nat. Chem*., 2009, **1**, 403.
41 Y. Li, H. Chen, L.Y. Voo, J. Ji, G. Zhang, G. Zhang, F. Zhang and X. Fan, *J. Mater. Chem*., 2012, **22**, 15021.
42 D.W. Chang, K.E. Lee, E.Y. Park, H. Yu, H.-J. Choi, I.-Y. Jeon, G.-J. Sohn, D. Shin, N. Park, J.H. Oh, L. Dai and J.-B. Baek, *J. Am. Chem. Soc*., 2013, **135**, 8981.
43 S.A. Bhat, M.A. Rather, S.A. Pandit, P.P. Ingole and M.A. Bhat, Analyst, 2015, **140**, 5601.
44 W. Shao, X. Liu, H. Min, G. Dong, Q. Feng and S. Zuo, *ACS Appl. Mater. Interfaces*, 2015, **7**, 6966.
45 G. Liu, Y. Wang, X. Pu, Y. Jiang, L. Cheng and Z. Jiao, *Appl. Surf. Sci.*, 2015, **349**, 570.
46 B. Sharma, R.R. Frontiera, A.-I. Henry, E. Ringe and R.P.V. Duyne, *Mater. Today*, 2012, **15**, 16.

Dalton Transactions Accepted Manuscript

Graphical Abstract

One-pot environmental friendly amino acid mediated synthesis of N-doped graphene-silver nanocomposites with enhanced multifunctional behavior

Mahima Khandelwal and Anil Kumar*

Department of Chemistry, Indian Institute of Technology Roorkee, Roorkee-247667, India.
E-mail: anilkfcy@iitr.ac.in; akmshfcy@gmail.com

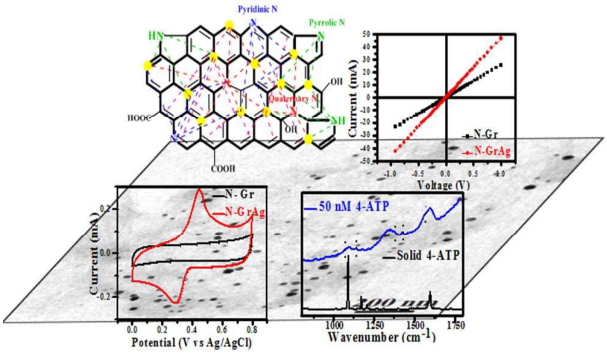

N-doped graphene-Ag nanocomposites having Ag bound supramolecularly through different N-Gr domains exhibit enhanced surface area, electrical, electrochemical and SERS activity.

Dalton Transactions Accepted Manuscript